Earth and Planetary Science Letters 270 (2008) 200–208

Contents lists available at ScienceDirect

Earth and Planetary Science Letters

journal homepage: www.elsevier.com/locate/epsl

Ferromagnetic resonance and magnetic characteristics of intact magnetosome chains in *Magnetospirillum gryphiswaldense*

Håkon Fischer [a,*], Giovanni Mastrogiacomo [b], Jörg F. Löffler [b], Rolf J. Warthmann [c], Peter G. Weidler [d], Andreas U. Gehring [a]

[a] *Institute of Geophysics, ETH Zurich, 8093 Zurich, Switzerland*
[b] *Laboratory of Metal Physics and Technology, Department of Materials, ETH Zurich, 8093 Zurich, Switzerland*
[c] *Geological Institute, ETH Zurich, 8092 Zurich, Switzerland*
[d] *Forschungszentrum Karlsruhe, Institute for Technical Chemistry, Water- and Geotechnology, 76021 Karlsruhe, Germany*

ARTICLE INFO

Article history:
Received 12 October 2007
Received in revised form 11 February 2008
Accepted 4 March 2008
Available online 18 March 2008

Editor: G.D. Price

Keywords:
magnetosomes
mon-stoichiometry
FMR spectroscopy
anisotropy
electron hopping

ABSTRACT

The magnetic characteristics of intact magnetosome chains in *Magnetospirillum gryphiswaldense* bacteria were investigated by means of static and dynamic magnetic analyses and ferromagnetic resonance spectroscopy. The nano-sized magnetosomes are generally in a stable single-domain state, but magnetosomes smaller than 30 nm characteristic of superparamagnetic magnetite particles were also found. Alternating current (AC) susceptibility indicates that all magnetosomes are blocked below 150 K. At room temperature the anisotropy of *M. gryphiswaldense* is dominated by the shape of the magnetosome chains. Low-temperature ferromagnetic resonance (FMR) spectroscopy indicates that this dominant shape anisotropy can affect the detection of the Verwey transition at 100 K. The static and dynamic magnetic analyses show that the Verwey transition is smeared and that our magnetotactic bacteria fail the Moskowitz test. This failure is explained by the biomineralization of non-stoichiometric magnetosomes. This interpretation is based on the increase in high-field susceptibility and the distinct peak in the out-of-phase component of the AC susceptibility below 50 K. These results are attributed to freezing of spins associated with defect structures in the core and at the surface of nano-sized magnetosomes. The results obtained from *M. gryphiswaldense* demonstrate that intrinsic properties of nano-sized magnetosomes are significantly influenced by non-stoichiometry and by the anisotropy excited from their arrangement in the bacteria.

1. Introduction

Magnetotactic bacteria were first discovered about 30 yr ago (Blakemore, 1975). Since then various species from lacustrine, terrestrial and marine environments have been described (e.g. Paasche et al., 2004; Fassbinder et al., 1990; Petersen et al., 1986). Only a few wild-type bacteria have been cultured in the laboratory (Flies et al. 2005). Prominent among these is *Magnetospirillum gryphiswaldense*, which was first found in the river Ryck near Greifswald, Germany (Schüler, 2002).

Magnetotactic bacteria possess the ability to form intercellular stable single-domain (SSD) magnetite with a narrow range of grain sizes and shape distributions (Blakemore and Frankel, 1989). Smaller particles in the superparamagnetic range (<30 nm) have also been observed in association with magnetotactic bacteria (Pan et al., 2005a).

Magnetite particles enclosed in membranes are specified as magnetosomes; they are usually arranged in chains along their easy axes, i.e. the [111] direction (Simpson et al. 2005). The development of a genetic system for *M. gryphiswaldense* opened the door for microbiological investigation of the biomineralization of magnetosomes (Schultheiss and Schüler, 2003). Scheffel et al. (2006) pointed out that the alignment of the magnetosomes is a genetically-controlled process. It is generally assumed that the close alignment of magnetosomes in chains, which maximizes the magnetic moment felt by these motile bacteria, helps them to orient along the Earth's magnetic field while seeking optimal oxygen conditions (Blakemore and Frankel, 1981). It has also been suggested that intercellular iron could be used as energy storage for redox-cycling or iron homeostasis (Mann et al., 1990).

Magnetotactic bacteria can be easily identified under the transmission electron microscope (TEM) because of the alignment of uniformly-sized magnetosomes in chains. Transmission electron microscopy is a powerful tool for studying morphological and structural properties of selected numbers of magnetosomes, but it delivers only limited information about magnetotactic bacteria in bulk samples. In recent years several approaches have been developed to detect these organisms in bulk samples using specific magnetic properties of

* Corresponding author. Institute of Geophysics, ETH Zurich, 8093 Zurich, Switzerland.
E-mail address: hakon.fischer@mag.ig.erdw.ethz.ch (H. Fischer).

0012-821X/$ – see front matter © 2008 Elsevier B.V. All rights reserved.
doi:10.1016/j.epsl.2008.03.022

magnetite. An intrinsic property is known as the Verwey transition. On cooling through this transition, magnetite undergoes a structural change from cubic to monoclinic and magnetocrystalline anisotropy energy increases by one order of magnitude. In stoichiometric magnetite this transition occurs at about 120 K, and it is characterized by distinctive changes in magnetization and coercivity (e.g. Özdemir et al., 2002; Muxworthy and McClelland, 2000). The Verwey transition associated with magnetotactic bacteria often occurs at a lower temperature (T_v) around 100 K, and it has been suggested that the lower T_v is an intrinsic property (Pan et al., 2005a; Prozorov et al., 2007). Significant lowering of T_v to about 20 K has been reported for 50 nm nanoparticles (Goya et al., 2003), a size often found in magnetotactic bacteria (e.g., Prozorov et al., 2007). Recent reviews of the Verwey transition have shown that the physical details of this transition are still not fully understood (Walz, 2002; Garcia and Subias, 2004). Nevertheless, the empirical Moskowitz test (Moskowitz et al., 1993), which compares saturation isothermal remanent magnetization (SIRM) of magnetosomes above and below T_v, has been successfully applied as a magnetic proxy to detect magnetotactic bacteria cultured in the laboratory (Pósfai et al., 2005) and collected from recent sediments (Pan et al., 2005b). This test is based on two facts: that in the monoclinic magnetite phase magnetocrystalline anisotropy is much greater than in the cubic phase, and that the magnetosomes aligned in chains generate shape anisotropy. The Moskowitz test proposes that the relative magnitude of demagnetization upon warming across the Verwey transition after field and zero-field cooling conditions is indicative of magnetotactic bacteria. The failure of the test due to smearing or even absence of the Verwey transition has been generally explained by stoichiometric changes due to oxidation after the biomineralization of the magnetite (Moskowitz et al., 1993). The possibility that the Moskowitz test may fail as a result of intrinsic non-stoichiometry of the magnetosomes or because of other physical properties has not yet been clearly resolved.

Recently several authors have proposed ferromagnetic resonance (FMR) spectroscopy, which is sensitive to magnetic anisotropy, as a means of detecting magnetotactic bacteria (Weiss et al., 2004; Kopp et al., 2006a). They report that the FMR spectra of intact magnetotactic bacteria recorded at room temperature are dominated by shape anisotropy due to the alignment of magnetosomes in chains. The comparison of FMR spectra recorded at room temperature and 77 K shows that the anisotropy properties change significantly above and below T_v. These FMR data, however, provide no information on the effect of the anisotropy properties on the Verwey transition.

This study, which combines magnetic analysis and FMR spectroscopy, addresses the anisotropy properties and the effect of non-stoichiometry on the magnetization of magnetotactic bacteria in a temperature range between room temperature and 5 K. We used intact bacteria of the strain *M. gryphiswaldense* because their microbiological properties have been extensively studied (Schüler, 2002, 2004), they can be easily cultured in the laboratory, and they form equidimensional magnetosomes for which the cubic magnetocrystalline anisotropy is dominant. The magnetic and spectroscopic data reveal for the investigated magnetotactic bacteria a smeared Verwey transition with a temperature of about 100 K.

2. Samples and methods

The magnetotactic bacteria *M. gryphiswaldense* strain MSR-1, DSM 6361 obtained from the Deutsche Sammlung von Mikroorganismen und Zellkulturen GmbH (DSMZ), were grown in a medium described by Heyen and Schüler (2003) under micro-aerophilic conditions in 2.5 L batch cultures. For transmission electron microscopy (TEM) the bacteria were fixed in 3% glutaraldehyde/PBS for 2 h, washed and mixed into a compound with 2% agar. Pieces were cut, dehydrated in a graded series of ethanol and penetrated gradually with Epon 812 resin. After polymerization at 60 °C the blocks were trimmed and 60 nm sections were cut and transferred onto formvar/carbon-coated copper grids. The ultra-thin sections were analysed in a Philips CM200 FEG transmission electron microscope.

For the mineralogical, magnetic, and spectroscopic analyses the bacteria were freeze-dried. The mineralogical properties of the magnetosomes were determined by X-ray diffraction (XRD) on a PANalytical X'Pert Pro apparatus, with Cu-K $_{\alpha 1}$ radiation over a 2θ range of 15° to 65° with 80 s per 0.02° step. The sample was fixed on a flat silicon plate with zero background. Using the Bragg equation for cubic systems, the lattice cell parameter a_0 was determined by extrapolation of a parameters calculated from each hkl reflections and $\cot(\theta)/\sin(\theta)$ against $\theta=90°$. The details of this procedure are described elsewhere (Klug and Alexander, 1975). The cation deficiency Δ for the magnetosomes ($Fe_{3(1-\Delta)}O_4$) was deduced by applying Vegard's rule using the lattice cell parameters for maghemite ($Fe_{2.66}O_4$) with $\Delta=0.11$ and magnetite with $\Delta=0$ as end-members.

A vibrating sample magnetometer (VSM, Princeton Instruments) was used to measure the magnetic moment ($V\times M$, where M is the magnetization and V the unknown volume) in an applied field (B) of the sample between 60 K and 293 K during stepwise warming. The hysteresis loops were recorded while sweeping the external field (sweeping mode) starting in a 1 T field. The coercivity (B_c), the remanent magnetic moment ($V\times M_r$, where M_r is the remanent magnetization) and the saturation magnetic moment ($V\times M_s$, where M_s is the saturation magnetization) were determined. In addition, the coercivity of remanence (B_{cr}) was determined at room temperature, 130 K, 100 K and 77 K. The saturating field was 500 mT and the measurements were made with a 5 mT increment.

In addition, hysteresis loops in fields up to 5 T and high-field magnetization curves up to 9 T while stepping the external field (persistent mode) were conducted between 150 K and 10 K using a Quantum Design PPMS 9 magnetometer. Hysteresis loops at 20 K in zero-field-cooled (ZFC) and field-cooled (FC in a 1 T field) modes were recorded.

First-order reversal curve (FORC) diagrams were generated via measurements performed at room temperature. A FORC diagram is derived from repeated measurement of $M(B)$ curves, by which, in addition to the major hysteresis cycle, minor loops (113 in this study) between a saturating positive field of 1 T and a number of reversed fields are measured. In a FORC diagram, the horizontal axis denotes the coercive field B_c and is indicative of the grain size range, whereas the field B_b plotted on the vertical axis indicates magnetic interactions. A detailed description of the method can be found elsewhere (Roberts et al., 2000). The data were analysed with a Matlab code (M. Winklhofer, personal communication, 2006).

In order to estimate the characteristics of the magnetic interaction in the bulk sample, a Henkel plot at 130 K was determined. At this temperature the requirement of unaxial anisotropy is fulfilled, such that the Stoner–Wohlfarth model for non-interacting particles can be used. Starting from the AC demagnetized state, an isothermal remanent magnetization (IRM) was imparted to the sample in a weak DC field. After measurement of the IRM, the sample was AC demagnetized completely. A stronger field was applied and the new IRM measured. This step-by-step procedure was repeated until saturation IRM was achieved. Next, DC demagnetization of saturation IRM was observed. The sample was given saturation IRM in a 1 T field, after which a field was applied in the reverse direction and the ensuing remanent magnetization was measured. The sample was again saturated and the procedure repeated with ever stronger reverse fields until the sample was saturated in the reverse field direction. These experiments were performed on a Quantum Design PPMS 9 magnetometer.

The same instrument was used for the saturation isothermal remanent magnetization (SIRM) conducted in a field-cooled and zero-field-cooled mode. In the latter mode the ZFC sample was magnetized in a 2.5 T field at 10 K and subsequently warmed in a zero field up to room temperature in steps of 5 K. In the FC mode, in contrast, the

sample was exposed to a 2.5 T field upon cooling. The SIRM data were used for the delta–delta test of Moskowitz et al. (1993) which quantifies the enhancement of the FC and ZFC curves below T_v, by defining the δ_{fc}/δ_{zfc} ratio where $\delta = M_{80\ K} - M_{150\ K}/M_{80\ K}$.

The dynamic magnetization behavior of the sample was measured by means of AC susceptibility. The in-phase (χ') and the out-of-phase susceptibility (χ'') were recorded at different amplitudes (B_{ac}) between 0.1 and 1.2 mT and frequencies in the range from 200 Hz to 10 kHz.

For the FMR experiments freeze-dried intact magnetotactic bacteria were fixed in the glass tube with paraffin. The FMR spectra at room temperature were recorded on a Bruker EMX at a microwave frequency of 9.8 GHz, with a power of 0.06 mW, modulation amplitude of 0.1 mT, and a modulation frequency of 100 kHz. The angular dependence of the FMR spectra was determined by rotating the glass tube with a goniometer mounted on the top of the cavity. For the low-temperature experiment a Miniscope MS spectrometer was used with microwave frequency of 9.4 GHz, a power of 0.2 mW, and modulation amplitude of 0.2 mT. The FMR spectra were recorded after cooling the sample in the spectrometer cavity exposed to a 250 mT field. Because of the spectrometer design, the measurement at 77 K was conducted in a special dewar, after cooling the sample from 295 K to liquid nitrogen temperature in a 250 mT field.

For all FMR spectra, the effective resonance field (B_{eff}), the corresponding effective g-value (g_{eff}), and the linewidth δB were determined (Fig. 7a). The B_{eff} is defined as the field of zero-crossing in the derivative spectrum (Weiss et al., 2004; Okamura et al., 1952). The effective g-value (g_{eff}) was derived from B_{eff} using the resonance relation $g_{eff} = h\nu/\mu_B B_{eff}$, where h is Planck's constant (6.626×10^{-34} Js), ν is the microwave frequency, and μ_B is Bohr's magneton (9.274×10^{-24} J/T) (Wertz and Bolton, 1972). In addition, the FMR data were classified by subdividing the spectra into a low-field side defined by an applied field $B<B_{eff}$, and the high-field side with $B>B_{eff}$ (Griscom, 1974).

The simulation of the FMR spectra was performed using the Matlab code written by Kopp et al. (2006b) for cubic or uniaxial systems or a linear combination of the two. The congruence of the experimental and simulated spectra was maximized by a non-linear least-square fitting procedure (Kopp et al., 2006b).

3. Results

3.1. Structural and morphological properties

Inspection of the sample under the TEM revealed intact chains of about 1 μm in length containing about 20 to 25 magnetosomes (Fig. 1). The individual particles were nearly equidimensional and exhibited an average diameter of 35±5 nm. Some smaller particles (diameter<30 nm) were found. Given the millions of bacteria in the sample, however, the grain size information reflects an estimate and not a statistical value. The spacing between magnetosomes in chains was less than 10 nm, whereas the spacing between chains was more than an order of magnitude larger. X-ray diffractometry of the bulk samples at RT showed a cubic phase with $a_0 = 0.83945 \pm 0.00001$ nm. The best congruence of the diffractogram pattern was obtained with the data for magnetite published by Wright et al. (2002). Apart from the peaks assigned to magnetite, no additional peaks were found. For the magnetosomes a cation deficiency Δ of 0.01 was deduced from the lattice cell parameter a_0.

Fig. 1. TEM micrograph of intact *M. gryphiswaldense* bacteria with intercellular chains of magnetite nanoparticles.

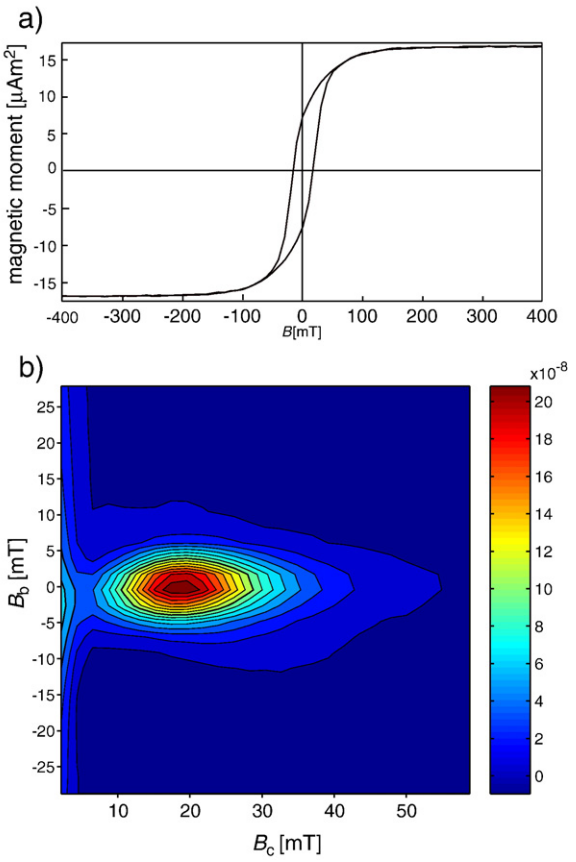

Fig. 2. Magnetic moment versus applied field (a) and FORC diagram (b) from the bulk sample of intact bacteria at RT; scale bar indicates the FORC distribution.

3.2. Magnetic measurements

3.2.1. Static magnetization

At room temperature, the magnetic moment against applied field (B), measured in sweeping mode, showed hysteretic properties for the magnetotactic bacteria with a coercivity (B_c) of 16.3 mT (Fig. 2a). The remanent magnetic moment was 7.44 μAm^2 and the saturation magnetic moment at 1 T was 16.91 μA m^2. The measured coercivity of remanence (B_{cr}) was 20.3 mT. Further, the remanence ratio M_r/M_s was 0.44 and the coercivity ratio B_{cr}/B_{cr} was 1.25 were obtained (Table 1). The

Table 1
Hysteresis and FMR spectral parameters at selected temperatures; the difference in the measuring temperatures of the hysteresis loops and FMR spectra (130 K/100 K in the hysteresis loops and 133 K/103 K in the FMR spectra) is indicated by 130/3 and 100/3

T (K)	"M_r" (μA m^2)	"M_s" (μA m^2)	M_r/M_s	B_c (mT)	B_{cr} (mT)	B_{cr}/B_c	δB (mT)	g_{eff}
295	7.44	16.91	0.44	16.27	20.34	1.25	185.6	1.867
130/3	7.94	17.29	0.46	18.67	23.86	1.28	164.4	1.951
100/3	7.93	17.09	0.46	18.10	23.75	1.31	159.9	2.029
77	8.52	16.98	0.50	23.06	29.65	1.29	198.1	2.218

"M_r" and "M_s" indicate M for an unknown volume, i.e. magnetic moment.

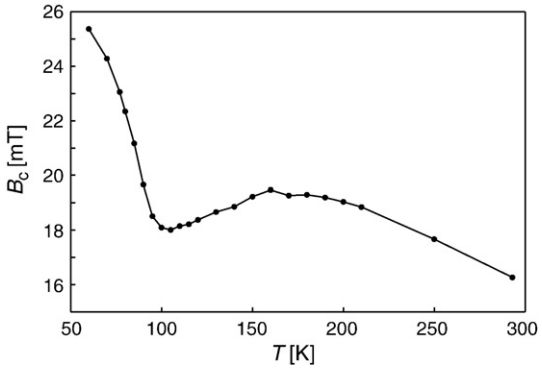

Fig. 3. Temperature behavior of the coercive field B_c between RT and 60 K.

FORC diagram at room temperature displayed two features (Fig. 2b). The dominant feature spread along B_c, with a maximum at 19 mT and a relative narrow distribution along the B_b axis. The interaction field was 7.4 mT as defined by the full width at half maximum of B_b distribution along a profile through the peak of the FORC distribution (Muxworthy and Dunlop, 2002). The second feature spread along the B_b axis, and B_c was smaller than 2 mT.

Upon cooling to 60 K, the temperature behavior of B_c could be divided into three ranges (Fig. 3). Between 295 K and 160 K an increase from 16.3 to 19.5 mT was observed, followed by a local minimum at 105 K with B_c=18 mT. At lower temperatures, an increase was observed with B_c=23.1 mT at 77 K (Table 1). The remanence ratio M_r/M_s increased to 0.46 upon cooling to 200 K and remained stable down to 95 K. Below this temperature, a steep increase was found, and at 77 K M_r/M_s was 0.5.

To detect further structural changes, high-field magnetization experiments up to 9 T were performed. Down to 70 K the slope of the high-field susceptibility was negative due to the diamagnetic contribution of the organic matrix. Between 70 and 40 K the slope of the high-field susceptibility at $B>0.3$ T became positive, indicating that the high-field component of the magnetosomes had become dominant. To saturate the sample at 10 K a magnetic field of about 7 T was required and M_s exhibited a strong increase (Fig. 4a). The contribution to M_s of the magnetization induced in $B>0.5$ T was about 50% of the magnetization induced in $B<0.5$ T. Hysteresis loops in a persistent mode revealed that the distinct increase in M_s occurred simultaneously with the doubling of B_c between 70 K and 10 K. The comparison of ZFC and FC hysteresis loops at 20 K exhibited neither a significant broadening nor a shift, but an increase of the remanent magnetic moment of about 20% upon field cooling (Fig. 4b) The FC and ZFC SIRM curve upon warming revealed kinks at about 100 K and less distinctly at about 45 K (Fig. 4c). In the FC curve these kinks were more pronounced. The δ_{fc}/δ_{zfc} ratio of 1.16 deduced from these curves clearly indicates that our *M. gryphiswaldense* failed the Moskowitz test, which generally yields a value of >2 for magnetotactic bacteria (Moskowitz et al., 1993). A ratio >2 was obtained if the low-temperature values of M were taken at 25 K.

The shape of the Henkel plot at 130 K (Fig. 5) deviated clearly from the ideal linear plot corresponding to Stoner–Wohlfarth conditions (Stoner and Wohlfarth, 1948). Two distinct departures were evident, at low and high fields, respectively.

3.2.2. Dynamic magnetization

In the temperature range between 295 K and 5 K the AC susceptibility measurements exhibited in-phase (χ') and out-of-phase (χ'') components (Fig. 6a and b). No amplitude dependence was found. By contrast, χ' revealed a frequency dependence over the whole temperature range. Upon cooling, χ' decreased and reached a local minimum at 250 K

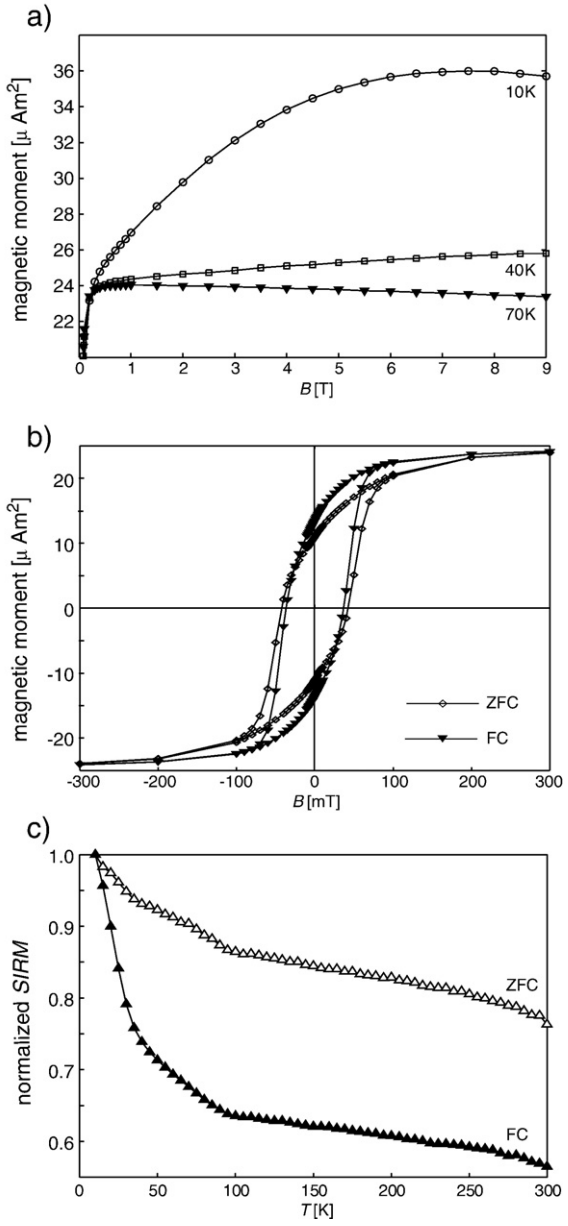

Fig. 4. High-field magnetization of the bulk sample at 10 K (circles), at 40 K (squares), and at 70 K (triangles) (a); hysteresis loops after ZFC (open diamonds) and after FC to 20 K in a 1 T field (solid triangles) (b); normalized ZFC (open triangles) and FC (solid triangles) SIRM curves (c).

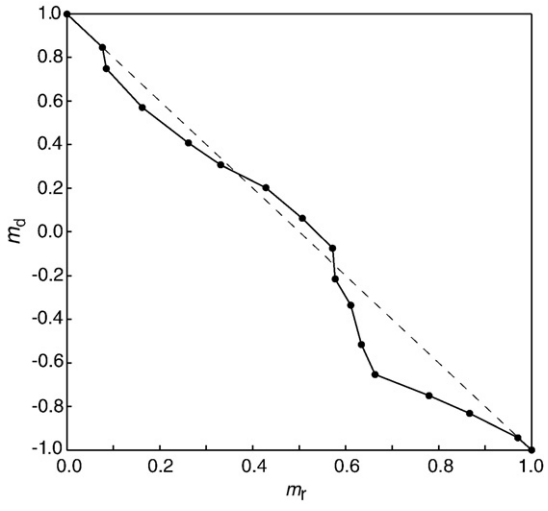

Fig. 5. Henkel plot at 130 K with the normalized demagnetization remanence (m_d) versus the normalized initial remanence (m_r) and the Stoner–Wohlfarth line characteristic of non-interacting particles.

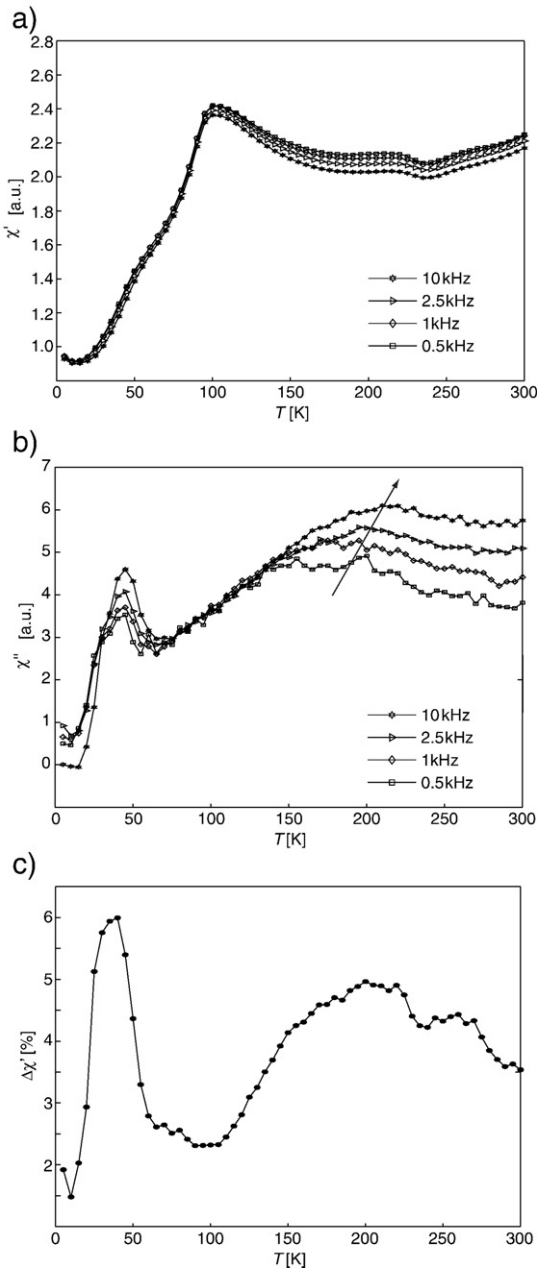

Fig. 6. Temperature dependence of the in-phase susceptibility χ' (a) and the out-of-phase susceptibility χ'' (b) measured with variable frequencies and an amplitude of 0.3 mT; the shift of the peak in χ'' is indicated by an arrow; (c) displays the frequency dependence of χ' expressed as $\Delta\chi' = (\chi'_{0.5\ \mathrm{kHz}} - \chi'_{10\ \mathrm{kHz}})/\chi'_{0.5\ \mathrm{kHz}}$ as a function of temperature.

followed by a moderate increase down to 100 K. At lower temperatures a drastic decrease in χ' was found with a kink at about 65 K. The amount of the frequency dependence $\Delta\chi' = (\chi'_{0.5\ \mathrm{kHz}} - \chi'_{10\ \mathrm{kHz}})/\chi'_{0.5\ \mathrm{kHz}}$ also changed with T (Fig. 6c). It increased between 295 K and 200 K and decreased down to 105 K, followed by a weak enhancement to 60 K and a pronounced peak at 40 K.

In the temperature range between 295 K and 150 K, broad peaks were observed in the out-of-phase component. Increasing AC frequency shifted this peak to a higher temperature. Between 150 K and 70 K no frequency dependence was detected. At lower temperatures a frequency-dependent local maximum was found at 45 K close to the peak of $\Delta\chi'$ (Fig. 6b and c).

3.3. FMR spectroscopy

At room temperature the FMR spectra displayed a line-shape with a sharp high-field and extended low-field absorption. The low-field side of the spectrum exhibited two positive peaks and a shoulder. The linewidth (δB) was 183.8 ± 0.4 mT and g_{eff} was found to be 1.885 ± 0.007 (Fig. 7a). The g_{eff} and to a minor extent δB revealed a weak angular dependence. The maximum and the minimum values of g_{eff} varied by about 1% and were separated by 90°. In addition, the maximum of g_{eff} occurred simultaneously with the maximal height of the peak at lower resonance and the minimal height of the peak at higher resonance (Fig. 7b). It is well-established that a maximal g_{eff} corresponds to the parallel alignment of the easy axes to an external field (Bickford, 1950; Fischer et al., 2007). The simultaneous maximum of g_{eff} and the peak at lower resonance point to chains with their easy axis oriented parallel to the applied field. The maximal and the minimal g_{eff} were also separated by 90°, and the minimal value coexisted with the maximum of the peak at higher resonance and the shoulder. Therefore, it is feasible to assign the peak at high resonance and the shoulder to chains with their easy axis perpendicular to the applied field. The presence of coupled features in the FMR spectra suggests collective properties of the magnetosomes in the chains. Moreover, the weak angular dependence of g_{eff} provides clear evidence that a preferential orientation of the magnetosome chains in the bulk sample is negligible.

Measurements at room temperature on the Miniscope spectrometer yielded $g_{\mathrm{eff}} = 1.867$ and $\delta B = 185.8$ mT. No significant changes in the spectral parameters were observed at RT after the low-temperature experiment. Upon cooling the line-shape revealed slight changes down to 133 K which are mainly characterized by the disappearance of the shoulder on the low-field side (Fig. 8). Between 133 and 103 K the peak at higher resonance became less pronounced. The low-temperature behavior of δB showed a slight increase down to 243 K and a pronounced decrease of 30 mT between 213 and 133 K (Fig. 9a). At lower temperatures the decrease became shallower and at 103 K δB was 160 mT. The decrease of δB accompanied the shift of the peak at lower resonance to

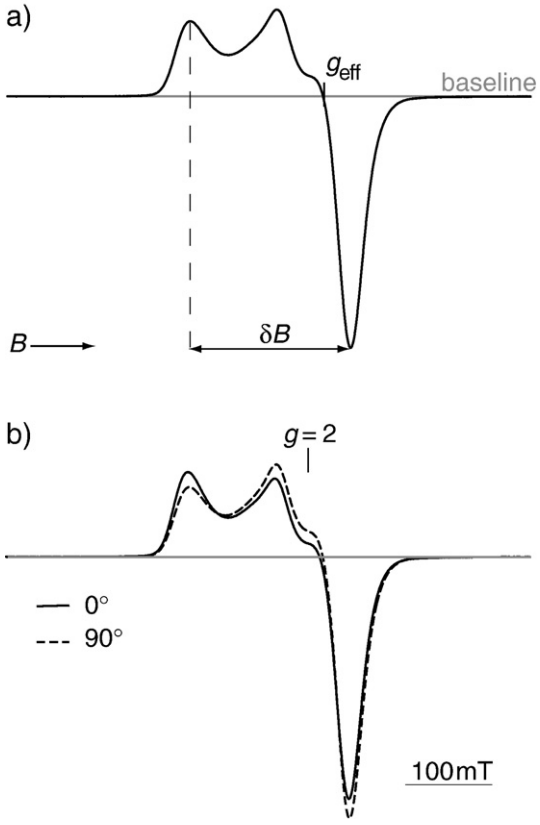

Fig. 7. Room temperature FMR spectrum of *M. gryphiswaldense* (recorded with a Bruker spectrometer), the baseline, effective g-value, (g_{eff}), linewidth δB and the external field B are indicated. (a); Superposition of two spectra with maximal variations of the height of the low-field peaks.(b).

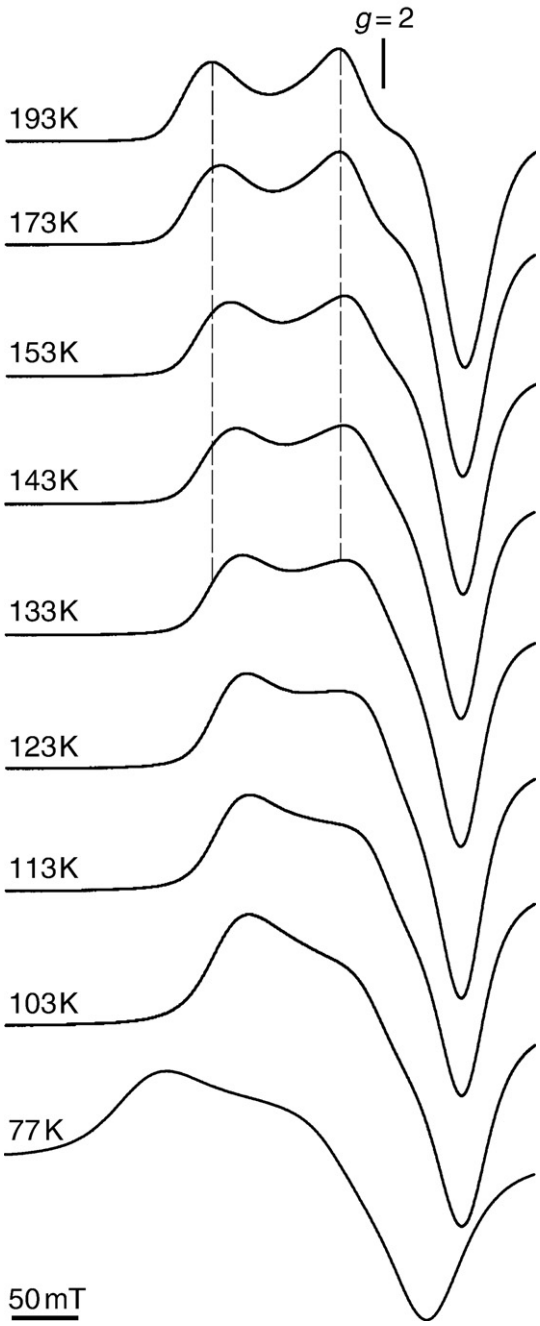

Fig. 8. Low-temperature FMR spectra recorded with a Miniscope spectrometer; the dashed line indicates the evolution of the two low-field peaks upon cooling to the isotropic temperature at about 133 K.

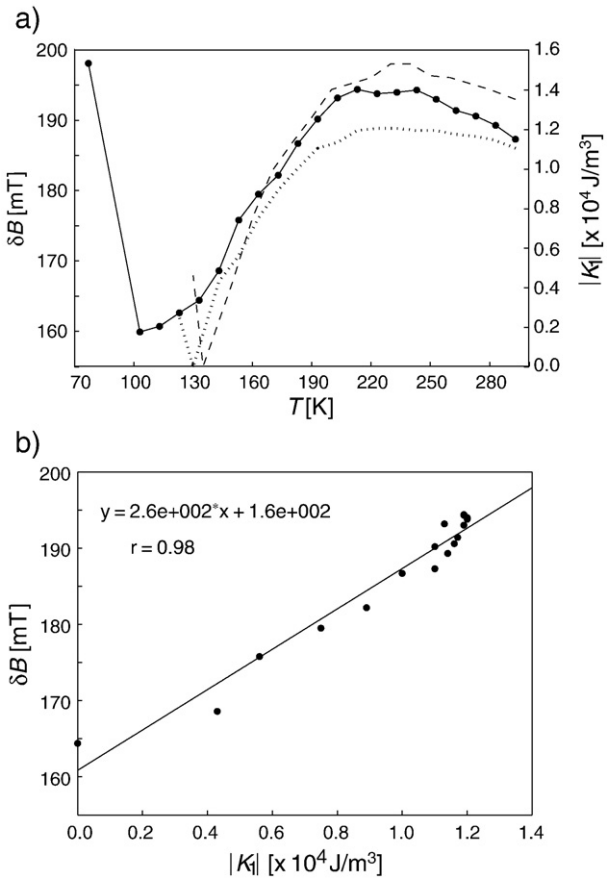

Fig. 9. Comparison of the low-temperature behavior of δB with $|K_1|$ (absolute values); K_1 is taken from Bickford et al. (1957) (short-dashed line) and from Syono and Ishikawa (1963) (long-dashed line) (a). Correlation between δB and $|K_1|$ taken from Bickford et al. (1957) (b).

higher fields, whereas the peak at higher resonance showed only slight changes (Fig. 8). Between 295 K and 133 K the shift of the peak at lower fields was 10%, similar to the change of δB, which was 12%.

In addition, the change of δB between RT and 133 K was similar to the development of the first-order magnetocrystalline constant K_1. A correlation coefficient between δB and K_1 of 0.98 was calculated (Fig. 9b). The g_{eff} values increased steadily from 1.885 at RT to 1.995 at 113 K. At $T<113$ K, g_{eff} even showed values of more than 2; at 77 K, g_{eff} was 2.218 and δB was 198 mT. To our knowledge, $g_{eff}<2$ for SSD magnetite powder sample has been reported only for magnetosomes in chains of intact bacteria (Weiss et al., 2004; Kopp et al., 2006a). The shift of g_{eff} to higher fields indicates a relatively strong internal field with demagnetizing properties that had to be compensated by the external field to reach resonance conditions. The value of $g_{eff}>2$ below 113 K hints to a decrease in this demagnetization effect (Fig. 8).

In the FMR simulation using the code written by Kopp et al. (2006b) it was not possible to reproduce all traits of the spectrum at room temperature. In contrast, using $K_1 \approx 0$ a reasonably good fit was obtained between experimental and simulated spectra at 133 K by considering only a uniaxial system (Fig. 10). The best fit yielded $g_{eff}=1.93$ and $\delta B=150$ mT.

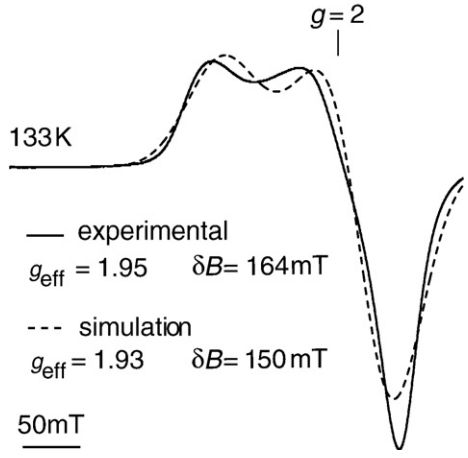

Fig. 10. Comparison of the measured and the simulated FMR spectrum at 133 K.

4. Discussion

The following discussion of the magnetic properties of the magnetosome chains in *M. gryphiswaldense* is subdivided into three parts. First, the blocking behavior of magnetosomes is addressed. The second part examines the anisotropy fields generated by the magnetosomes. In the third part we consider the magnetic properties of the magnetosomes at $T<100$ K, below the Verwey transition.

4.1. Grain size distribution and blocking above 100 K

The magnetosomes in this study exhibit similar morphology and size to those reported for magnetite particles generated in cultured strains of *M. gryphiswaldense* (Lang et al., 2007). This similarity corresponds to the well-established finding that magnetotactic bacteria of a specific species generate magnetosomes with a narrow size and shape distribution (Blakemore and Frankel, 1989). In our bulk sample the nanoparticles, are embedded in organic matter with diamagnetic properties. Most of the magnetosomes are arranged in chains (Fig. 1). This arrangement can be considered as an interacting system of nanoparticles. Our magnetosomes generally show diameters of about 35 nm but smaller particles of less than 30 nm are also observed (Fig. 1). The larger particles are unambiguously in the SSD size range, whereas the smaller magnetosomes are close to the threshold between blocked and superparamagnetic (SP) states (Dunlop and Özdemir, 1997). In a Day-plot (M_r/M_s versus B_{cr}/B_c) the bulk of the magnetosomes are located close to the field characteristic for uniaxial SSD magnetite (Day et al. 1977). The spread along the B_b axis at $B_c<2$ mT in the FORC diagram can be interpreted as caused by particles in SP state (Roberts et al., 2000). This interpretation is supported by the increase in B_c upon cooling to 160 K. Moreover, the shift of the out-of-phase susceptibility χ'' with increasing frequency at about 175 K (Fig. 6b) confirms that the smaller magnetosomes exhibit SP-like behavior. These magnetosomes are blocked at about 150 K, as indicated by the disappearance of the frequency dependence of χ'' below this temperature. Blocking leads to a broader grain size distribution of SSD magnetite at $T<150$ K compared to RT.

4.2. Magnetosomes and their anisotropy fields

Ferromagnetic resonance spectra of intact magnetotactic bacteria at RT are the results of a combination of anisotropy fields generated by magnetocrystallinity, shape and interactions Kopp et al. (2006b). The contribution of the various anisotropies to a FMR spectrum has not been examined in detail until now, either experimentally, comparing intact and clumps of magnetotactic bacteria, or in FMR simulations. In the following the qualitative contributions of different anisotropy fields to the absorption spectra at low temperatures are discussed.

The departure from the Stoner–Wohlfarth line of non-interacting, uniaxial SSD particles in the Henkel plot at 130 K suggests that the interactions in our sample have mainly demagnetizing properties. Demagnetization can be caused by magnetostatic interactions between single magnetosomes. Moreover electron holography analysis clearly showed that the alignment of magnetosomes generates a stray field, i.e. demagnetizing properties. With this in mind it is likely that the magnetic behaviour observed for *M. gryphiswaldense* is dominated by dipole characteristics arising from the geometric arrangement of the magnetosomes in the cell, i.e. by the uniaxial shape originated from entire chain. This is supported by the FMR spectrum at RT with its extended low-field and sharp high-field absorption typical for magnetic phase with uniaxial positive anisotropy properties (Griscom, 1974). The failure to simulate all features of the spectrum at RT using the code of Kopp et al. (2006b) indicates, that the magnetosome chains cannot be described solely in terms of a uniaxial system. Magnetite has cubic magnetocrystalline anisotropy with a negative K_1 between RT and the isotropic point near 130 K (Bickford et al. 1957; Syono and Ishikawa, 1963). The high correlation coefficient of 0.98 for δB and K_1 in the temperature range between RT and 133 K (Fig. 8a and b) indicates that the magnetocrystalline anisotropy field (B_m) contributes significantly to the absorption spectrum. The effect of B_m is supported by the low-temperature variation of the hysteresis parameter B_c (Morrish and Watt, 1958). Considering the above argumentation, the anisotropy field (B_a) in the bulk sample can be treated schematically as the sum of the magnetocrystalline anisotropy fields B_m of each particle and of the stray fields generated by aligned magnetosomes which can be considered as shape anisotropy field (B_s). In addition, B_a is assumed to be proportional to δB (Griscom, 1974).

Comparing the FMR spectra at RT and the isotropic point at 133 K provides an insight into the anisotropy properties of the bulk sample. In this temperature range, where B_m decreases by 100%, B_a is reduced by 12%. Thus B_m makes only a minor contribution to the anisotropy properties of the bulk sample. One has to be aware, however, that in the same temperature range B_s increases because of the increase in M_s. Using the relation $M_s(T)\propto(1-T/T_c)^{\gamma}$ with the Curie temperature T_c and $\gamma=0.43$ for magnetite, an enhancement of about 13% can be calculated for M_s (Dunlop and Özdemir, 1997). Therefore it can be argued that the less-pronounced decrease in B_a compared to B_m is a consequence of the changes in B_s.

The Henkel plot at 130 K reveals demagnetizing properties for the bulk sample. Demagnetization generally increases the resonance field B_{eff} and as a result decreases the g_{eff} value (Vonsovskii, 1966). Bickford (1950) reported a g-value of 2.08 for single-crystal magnetite at the isotropic point. Comparing this value with $g_{eff}=1.95$ obtained in our sample, a distinct contribution of B_s to B_a may be postulated.

Between 130 K and 100 K, the decrease in B_a indicates a diminishing of the anisotropy field acting on the spins localized with Fe. Since the change in B_a occurs simultaneously with the increase in B_m, it follows that B_s also decreases. An explanation for the reduction of B_s may be the shifting of the magnetic easy axes in the magnetosomes from [111] to [100] below the isotropic point at about 130 K. This departure of the easy axes from the chain axes weakens the dipole interactions of the magnetosomes, and subsequently B_s. Evidence for such an effect is apparent in the smearing out of the two resonance peaks in the FMR spectra between 130 K and 100 K (Fig. 8). The concomitant decrease in B_a and B_s between 133 K and 100 K suggests that this masks the change in B_m in this temperature range. The vanishing of the two peaks in the FMR spectra at 77 K, however, indicates that the major contribution to B_a below 100 K arises from B_m. The behavior of B_m agrees well with the increase in B_c and M_r/M_s, as well as the SIRM increase and the drop in χ'. Such changes in the magnetic parameters have been interpreted as characteristics of the Verwey transition (Özdemir et al., 2002; Kosterov, 2003).

4.3. Magnetic behavior of the magnetosomes below 100 K and the Verwey transition

Extensive studies on single crystals and magnetite powder have shown a Verwey transition at a temperature (T_v) near 125 K, which is about 10 K below the temperature of the isotropic point (T_i) of magnetite (Walz, 2002). Our hysteresis and SIRM data, however, indicate that the Verwey transition found for *M. gryphiswaldense* is smeared and shifted by about 20 K to a lower temperature. A Verwey transition at about 100 K has been observed for magnetosomes in various bacteria (Pan et al., 2005a; Prozorov et al., 2007; Weiss et al., 2004). Pan et al. (2005a) mentioned that the low T_v may be an intrinsic property of magnetosomes. Off-axes holography of magnetotactic bacteria (Simpson et al., 2005) reveals that despite some undulation of the magnetic induction below the isotropic point due to tilting of the easy axes, there is still magnetic coherence between the magnetosomes. This agrees well with the dominance of B_s indicated by FMR spectral data. Therefore the occurrence of the Verwey

transition at a lower temperature of about 100 K in magnetotactic bacteria may be affected by the persistence of the distinct contribution of B_s below the isotropic point.

The smearing of the Verwey transition has been explained by oxidation processes (Özdemir et al., 1993) or by cation substitution (Kakol et al., 1992). The latter can be neglected in the present case because the culture medium contains no cations which can substitute $Fe^{(II)}$ or $Fe^{(III)}$ in the magnetite lattice. Özdemir et al. (1993) compared non-oxidized and oxidized nano-sized inorganic magnetite powders and found that the departure from stoichiometry due to oxidation leads to drastic maghemitization and a subsequent gradient of the chemical composition between core and surface, which results in the smearing out of the Verwey transition. In oxidized magnetosomes Moskowitz et al. (1993) found an increase in SIRM at $T<50$ K and interpreted this as blocking of small SP maghemite particles. Taking these findings into account, the magnetic behavior of *M. gryphiswaldense* at low temperatures could be explained by maghemitization of the magnetosomes. The XRD data, however, provide no indication of maghemite in our bulk sample at RT and the FMR spectra do not show evidence for SP maghemite (Gehring et al., 1990). Blocking of maghemite as a low-coercivity phase similar to magnetite cannot explain the high-field susceptibility of the magnetization curve, which occurs simultaneous to the increase in SIRM. According to the above argumentation, maghemitization is unlikely to explain the low-temperature behavior of the magnetosomes.

Recently Faivre et al. (2007) found evidence for a ferritin-type compound in the membrane fraction of *M. gryphiswaldense*. Ferritin consists of an antiferromagnetic ferrihydrite ($5Fe_2O_3{\cdot}9H_2O$) nanoparticle surrounded by a protein shell (Chasteen and Harrison, 1999). It is known that the blocking temperature of ferritin is below 20 K (Brem et al. 2006; Seehra and Punnoose, 2001). Since no peaks are found in the AC susceptibility in this temperature range, a significant contribution of ferritin compounds to the low-temperature behavior in our sample is ruled out. Hence, the magnetic behavior at $T<50$ K is probably due to magnetite. This explanation is supported by the similarity of ZFC and FC hysteresis loops at 20 K; no broadening or shift of the loops are observed, which is therefore not consistent with exchange coupling of magnetite with an antiferromagnetic phase (Nogués and Schuller, 1999). Moreover, if an additional antiferromagnetic phase (e.g. ferrihydrite) causes the strong increase in the high-field susceptibility at $T<40$ K (Fig. 4a) it should be present in XRD-detectable quantities in the bulk sample.

At low temperatures, the magnetite structure undergoes a rearrangement of electronic states in regions with inhomogeneous spin distributions (Kronmüller and Walz, 1980). Muxworthy and McClelland (2000) and references therein reported that decreasing temperature leads to a more pronounced Vonovskii exchange interaction between the localized inner electrons and the valence electrons of Fe cations. Ordering of the valence electrons generates the formation of e-sublattices which are antiferromagnetically coupled to B-sites of the spinel crystal structure with octahedrally-coordinated Fe^{3+} and Fe^{2+}. The diminution of electron hopping due to ordering entails magnetic hardening of the material, since the A-sites of the magnetite with Fe^{3+} only become more pronounced. The high-field susceptibility and the doubling of B_c between 50 and 10 K indicate such a hardening effect in our magnetosomes. The temperature range in which this effect occurs accords with the finding by Kronmüller and Walz (1980), who demonstrated that below 45 K electron hopping ceases. Since it is known that an external field can destroy e-sublattices (Muxworthy and McClelland, 2000), an increase in remanent magnetic moment and a decrease in B_c are expected in the hysteresis loop after field cooling. The comparison of the ZFC and FC hysteresis loop at 20 K reveals just this effect (Fig. 4b). With this in mind, it can be postulated that the magnetic behavior (e.g. increase in SIRM and B_c) of the magnetosomes below 50 K is mainly affected by the ordering of electron spins in e-sublattices. Further evidence for the ordering of inhomogeneously-distributed electron spins is provided by the distinct frequency dependence of χ' and χ'' at about 50 K (Fig. 6b and c). Skumryev et al. (1999) showed that regions with inhomogeneous spin distributions could be domain walls, and that the frequency dependence is due to freezing out of defects and interstitials. The magnetosomes in this study, however, are of SSD size, and, therefore the inhomogeneity must occur within the grain core and its surface.

In a study of synthesized non-stoichiometric single magnetite crystals, Kakol and Honig (1989a) reported that a decreased T_v is caused by cation deficiency (Δ) in the magnetite structure ($Fe_{3(1-\Delta)}O_4$). Magnetite with $\Delta<0.01$ has a lower K_1 than pure magnetite, but shows a similar temperature dependence with an isotropic point T_i near 130 K (Kakol and Honig, 1989b). A Verwey transition is documented in the non-stoichiometric magnetite with $\Delta<0.012$ (Kakol and Honig, 1989a,b). The XRD data of *M. gryphiswaldense* reveal a Δ of 0.01. For such a value a T_v of ca. 90 K was reported (Kakol and Honig, 1989a), which is close to $T_v \approx 100$ K found for *M. gryphiswaldense* in this study. In contrast to the magnetite single crystal used by Kakol and Honig (1989a), the magnetosomes are in the nanometer range with large specific surface areas. Therefore it is feasible that the surfaces of the magnetosomes contribute significantly to the departure from stoichiometry. With this in mind, the magnetic behavior below the Verwey transition is most likely due to non-stoichiometry and subsequent rearrangement of electronic spins in the core and on the surface, and their freezing at $T<50$ K.

4.4. Non-stoichiometry in the magnetosomes

Non-stoichiometry in the context of magnetosomes has generally been taken to be an effect of maghemitization and has been used to explain relatively low δ-ratios (Moskowitz et al., 1993; Weiss et al., 2004). Despite their low δ-ratio, our magnetic and mineralogical data show no indication for oxidative alteration of the magnetosomes in *M. gryphiswaldense*. Hence it is feasible to argue that the non-stoichiometry in our case is the result of biomineralization. The details of the magnetite biomineralization are so far unresolved. Two processes can be suggested: the co-precipitation of Fe^{2+} and Fe^{3+} or formation via a ferrihydrite precursor. In the latter case the absorption of soluble Fe^{2+} would lead to the magnetite phase. High-resolution TEM data revealed twinning in magnetosomes, which suggests structural inhomogeneity in the nanoparticles (Devouard et al., 1998). Such inhomogeneity can be a growth phenomenon or the result of a phase transition. The latter possibility is supported by the detection of a ferritin-type compound in magnetosome membranes of *M. gryphiswaldense* (Faivre et al., 2007). Therefore it is probable that, during the mineral transition, defect structures such as vacancies can be produced. Based on our data, however, an unambiguous interpretation of the non-stoichiometry of the nano-sized magnetosomes remains elusive. Nevertheless, the magnetic characteristics of the magnetosomes provide clear evidence that non-stoichiometry in these nano-sized particles may be an intrinsic property.

5. Conclusion

The experimental approach in this study, which combines static and dynamic magnetization and FMR spectroscopy, shows a superposition of magnetic characteristics in the low-temperature range for magnetosomes of *M. gryphiswaldense* which are summarized as follows:

(1) At room temperature nano-sized magnetosomes aligned in chains, consist of single-domain and superparamagnetic magnetite nanoparticles. At 150 K all magnetosomes are blocked.
(2) Stray fields of the dipoles formed by magnetosome chains generate the anisotropy field B_s of the bacteria. This anisotropy field, dominant down to 100 K, masks the increase in B_m between the isotropic point and the Verwey transition in intact magnetotactic bacteria.

(3) Values of $g_{eff} < 2$ can be used as a proxy to detect magnetotactic bacteria even if they fail the Moskowitz test.
(4) The magnetic parameters indicate a Verwey transition of the magnetosomes at about 100 K. The smearing of the Verwey transition associated with *M. gryphiswaldense* is caused by non-stoichiometry in the core and at the surface of the nano-sized magnetosomes. The departure from stoichiometry and the subsequent inhomogeneous electron spin distribution in the single-domain magnetosomes can also explain the distinct static and dynamic magnetic behavior at $T<50$ K.
(5) The combined magnetic and spectroscopic information on the magnetosomes points to particular magnetic properties of biologically-controlled magnetite aligned in chains. Genetic information may be a key in linking the magnetic properties and the processes leading to biomineralization in cultured *M. gryphiswaldense*.

Acknowledgements

The authors are grateful to G. Jeschke and Y. Polyhach (Universität Konstanz) for their help with the low-temperature FMR measurements. We also thank A.G. Bittermann (Universität Zürich) for TEM sample preparation, P. Formanek (TU Dresden) for the TEM micrographs, Ch. Bärlocher (ETH Zürich) for the XRD data, and Bill Lowrie for his critical review. PGW would like to thank the Danish Research Council for Technology and Production for granting him a research stay at IGV (Faculty of Life Sciences, University Copenhagen) via grant no. 274-06-0053. This work was supported by ETH research grant TH02296. (Contribution 1517 of the Institute of Geophysics, ETH Zurich.)

References

Bickford, L.R., 1950. Ferromagnetic resonance absorption in magnetite single crystals. Phys. Rev. 78, 449–547.
Bickford Jr., L.R., Bronlow, J.L., Penoyer, R.F., 1957. Magnetocrystalline anisotropy in cobalt-substituted magnetite single crystals. Proc. IEEE B 104, 238–244.
Blakemore, R.B., 1975. Magnetotactic bacteria. Science 190, 377–379.
Blakemore, R.P., Frankel, R.B., 1981. Magnetic navigation in bacteria. Sci. Am. 245, 42–49.
Blakemore, R.P., Frankel, R.B., 1989. Magnetite and magnetotaxis in microorganisms. Bioelectromagnetics 10, 223–237.
Brem, F., Tiefenauer, L., Fink, A., Dobson, J., Hirt, A.M., 2006. A mixture of ferritin and magnetite nanoparticles mimics the magnetic properties of human brain tissue. Phys. Rev., B 73, 224427–1–224427-5.
Chasteen, N.D., Harrison, P.M., 1999. Mineralization in ferritin: an efficient means of iron storage. J. Struct. Biol. 126, 182–194.
Day, R., Fuller, M., Schmidt, V.A., 1977. Hysteresis properties of titanomagnetites: grain-size and compositional dependence. Phys. Earth Planet. Inter. 13, 260–267.
Devouard, B., Pósfai, M., Hua, X., Bazylinski, D.A., Frankel, R.B., Buseck, P.R., 1998. Magnetite from magnetotactic bacteria: size distributions and twinning. Am. Min. 86, 1387–1398.
Dunlop, D., Özdemir, O., 1997. Rock Magnetism: Fundamentals and Frontiers. Cambridge University Press, Cambridge, UK.
Faivre, D., Boettker, L.H., Schüler, D., Matzanke, B.F., 2007. Biosynthesis of magnetite in magnetosomes and the role of ferritin in *M. gryphiswaldense*. Am. J. Hematol. 82, 508–508.
Fassbinder, J.W., Stanjek, H., Vali, H., 1990. Occurrence of magnetic bacteria in soil. Nature 343 (6254), 161–163.
Fischer, H., Luster, J., Gehring, A.U., 2007. EPR evidence for maghemitization of magnetite in a tropical soil. Geophys. J. Int. 169, 909–916.
Flies, C.B., Jonkers, H.M., de Beer, D., Bosselmann, K., Böttcher, M.E., Schüler, D., 2005. Diversity and vertical distribution of magnetotactic bacteria along chemical gradients in freshwater microcosms. FEMS Microbiol. Ecol. 52, 185–195.
Garcia, J., Subias, G., 2004. The Verwey transition — a new perspective. J. Phys., Condens. Matter 16, R145–R178.
Gehring, A.U., Karthein, R., Reller, A., 1990. Activated state in the lepidocrocite structure during thermal treatment. Naturwissenschaften 77, 177–179.
Goya, G.F., Berquo, T.S., Fonseca, F.C., Morales, M.P., 2003. Static and dynamic magnetic properties of spherical magnetite nanoparticles. J. Appl. Phys. 94, 3520–3528.
Griscom, D.L., 1974. Ferromagnetic resonance spectra of lunar fines: some implications of lineshape analysis. Geochim. Cosmochim. Acta 38, 1509–1519.
Heyen, U., Schüler, D., 2003. Growth and magnetosome formation by microaerophilic *Magnetospirillum* strains in an oxygen-controlled fermentor. Appl. Microbiol. Biotechnol. 61, 536–544.
Kakol, Z., Honig, J.M., 1989a. The variation of Verwey transition temperature with oxygen stoichiometry in magnetite. Solid State Commun. 70, 967–969.
Kakol, Z., Honig, J.M., 1989b. Influence of deviations from the ideal stoichiometry on the anisotropy parameters of magnetite $Fe_{3(1-\delta)}O_4$. Phys.Rev., B 40, 9090–9096.
Kakol, Z., Sabol, J., Stickler, J., Honig, J.M., 1992. Effect of low-level titanium(IV) doping on the resistivity of magnetite near the Verwey transition. Phys. Rev., B 46 (4), 1975–1978.
Klug, H.P., Alexander, L.E., 1975. X-ray Diffraction Procedures. J. Wiley, New York.
Kopp, R.E., Weiss, B.P., Maloof, A.C., Vali, H., Nash, C.Z., Kirschvink, J.L., 2006a. Chains, clumps, and strings: magnetofossil taphonomy with ferromagnetic resonance spectroscopy. Earth Planet. Sci. Lett. 247, 10–25.
Kopp, R.E., Nash, C.Z., Kobayashi, A., Weiss, B.P., Bazylinski, D.A., Kirschvink, J.L., 2006b. Ferromagnetic resonance spectroscopy for assessment of magnetic anisotropy and magnetostatic interactions: a case study of mutant magnetotactic bacteria. J. Geophys. Res. 111.
Kosterov, A., 2003. Low-temperature magnetization and ac susceptibility of magnetite: effect of thermomagnetic history. Geophys. J. Int. 154, 58–71.
Kronmüller, H., Walz, F., 1980. Magnetic after effects in Fe_3O_4 and vacancy-doped magnetite. Philos. Mag., B 42, 433–452.
Lang, C., Schüler, D., Faivre, D., 2007. Synthesis of magnetite nanoparticles for bio- and nanotechnology: genetic engineering and biomimetics of bacterial magnetosomes. Macromol. Biosci. 7, 144–151.
Mann, S., Sparks, N.H., Board, R.G., 1990. Magnetotactic bacteria: microbiology, biomineralization, paleomagnetism and biotechnology. Adv. Microb. Physiol. 31, 125–181.
Morrish, A.H., Watt, L.A.K., 1958. Coercive force of iron oxide micropowders at low temperatures. J. Appl. Phys. 29, 1029–1033.
Moskowitz, B.M., Frankel, R.B., Bazylinski, D.A., 1993. Rock magnetic criteria for the detection of biogenic magnetite. Earth Planet. Sci. Lett. 120, 283–300.
Muxworthy, A., Dunlop, D., 2002. First-order reversal curve (FORC) diagrams for pseudo-single-domain magnetites at high temperature. Earth Planet. Sci. Lett. 203, 369–382.
Muxworthy, A.R., McClelland, E., 2000. Review of the low-temperature magnetic properties of magnetite from a rock magnetic perspective. Geophys. J. Int. 140 (1), 101–114.
Nogués, J., Schuller, I.K., 1999. Exchange bias. J. Magn. Magn. Mater. 192, 203–232.
Okamura, T., Torizuka, Y., Kojima, Y., 1952. The g factor of ferrites. Phys. Rev. 88, 1425–1426.
Özdemir, Ö., Dunlop, D., Moskowitz, B.M., 1993. The effect of oxidation on the Verwey transition in magnetite. Geophys.Res. Lett. 20, 1671–1674.
Özdemir, Ö., Dunlop, D., Moskowitz, B.M., 2002. Changes in remanence, coercivity and domain state at low temperature in magnetite. Earth Planet. Sci. Lett. 194, 343–358.
Paasche, Ø., Løvlie, R., Dahl, S.O., Bakke, J., Nesje, A., 2004. Bacterial magnetite in lake sediments: Late glacial to Holocene climate change and sedimentary changes in northern Norway. Earth Planet. Sci. Lett. 223, 319–333.
Pan, Y., Petersen, N., Winklhofer, M., Davila, A.F., Liu, Q., Friederichs, T., Hanzlik, M., Zhu, R., 2005a. Rock magnetic properties of uncultured magnetotactic bacteria. Earth Planet. Sci. Lett. 237, 311–325.
Pan, Y., Petersen, N., Davila, A.F., Liu, Q., Zhang, L., Winklhofer, M., Hanzlik, M., Zhu, R., 2005b. The detection of bacterial magnetite in recent sediments of Lake Chiemsee (southern Germany). Earth Planet. Sci. Lett. 232, 109–123.
Petersen, N., von Dobeneck, T., Vali, H., 1986. Fossil bacterial magnetite in deep-sea sediments from the South-Atlantic Ocean. Nature 320, 611–615.
Pósfai, M., Moskowitz, B., Arato, B., Schüler, D., Flies, C., Bazylinski, D.A., Frankel, R.B., 2005. Properties of intracellular magnetite crystals produced by *Desulfovibrio magneticus* strain RS-1. Earth Planet Sci. Lett. 249, 444–445.
Prozorov, R., Prozorov, T., Mallapragada, S.K., Narasimhan, B., Williams, T.J., Bazylinski, D.A., 2007. Magnetic irreversibility and the Verwey transition in nanocrystalline bacterial magnetite. Phys. Rev., B 76, 054406–1–054406-9.
Roberts, A.P., Pike, C.R., Verosub, K.L., 2000. First-order reversal curve diagrams: a new tool for characterizing the magnetic properties of natural samples. J. Geophys. Res. 105, 28461–28475.
Scheffel, A., Gruska, M., Faivre, D., Linaroudis, A., Plitzko, J.M., Schüler, D., 2006. An acidic protein aligns magnetosomes along a filamentous structure in magnetotactic bacteria. Nature 440, 110–114.
Schüler, D., 2004. Molecular analysis of a subcellular compartment: the magnetosome membrane in *Magnetospirillum gryphiswaldense*. Arch. Microbiol. 181, 1–7.
Schüler, D., 2002. The biomineralization of magnetosomes in *Magnetospirillum gryphiswaldense*. Int. Microbiol. 5, 209–214.
Schultheiss, D., Schüler, D., 2003. Development of a genetic system for *Magnetospirillum gryphiswaldense*. Arch. Microbiol. 179, 89–94.
Seehra, M.S., Punnoose, A., 2001. Deviations from the Curie-law variation of magnetic susceptibility in antiferromagnetic nanoparticles. Phys. Rev., B 64, 132410–1–132410-4.
Simpson, E.T., Posfai, M., Busek, P.R., Harrison, R.J., Dunin-Borkowski, R.E., 2005. Magnetic induction mapping of magnetite chains in magnetotactic bacteria at room temperature and close to the Verwey transition. J. Phys., Conf. Ser. 17, 108–121.
Skumryev, V., Blythe, H.J., Cullen, J., Coey, J.M.D., 1999. AC susceptibility of a magnetite crystal. J. Magn. Magn. Mater. 196–197, 515–517.
Stoner, E.C., Wohlfarth, E.P., 1948. A mechanism of magnetic hysteresis in. heterogeneous alloys. Philos. Trans. Lond. Ser. A 240, 599–642.
Syono, Y., Ishikawa, Y., 1963. Magnetocrystalline anisotropy of $x Fe_2TiO_4$ $(1-x)$ Fe_3O_4. J. Phys. Soc. Jpn. 18, 1230–1231.
Vonsovskii, S.V. (Ed.), 1966. Ferromagnetic Resonance. Pergamon Press, Oxford.
Walz, F., 2002. The Verwey transition — a topical review. J. Phys. Condens., Matter 14, R285–R340.
Weiss, B.P., Kim, S.S., Kirschvink, J.L., Kopp, R.E., Sankaran, M., Kobayashi, A., Komeili, A., 2004. Ferromagnetic resonance and low-temperature magnetic tests for biogenic magnetite. Earth Planet. Sci. Lett. 224, 73–89.
Wertz, J.E., Bolton, J.R., 1972. Electron Spin Resonance. McGraw-Hill, New York.
Wright, J.P., Attfield, J.P., Radaelli, P.G., 2002. Charge ordered structure of magnetite Fe_3O_4 below the Verwey transition. Phys. Rev., B 66, 214422.